

Incompressible two-phase flows with an inextensible Newtonian fluid interface



Sebastian Reuther^a, Axel Voigt^{a,b,c,*}

^a Institute of Scientific Computing, TU Dresden, 01062 Dresden, Germany

^b Dresden Center for Computational Materials Science (DCMS), TU Dresden, 01062 Dresden, Germany

^c Center for Systems Biology Dresden (CSBD), Pfotenhauerstr 108, 01307 Dresden, Germany

ARTICLE INFO

Article history:

Received 16 April 2016

Received in revised form 14 July 2016

Accepted 20 July 2016

Available online 26 July 2016

Keywords:

Interfacial fluids

Diffuse interface approximation

Lipid membranes

ABSTRACT

We introduce a diffuse interface approximation for an incompressible two-phase flow problem with an inextensible Newtonian fluid interface. This approach allows to model lipid membranes as viscous fluids. In the present setting the membranes are assumed to be stationary. We validate the model and the numerical approach, which is based on a stream function formulation for the surface flow problem, an operator splitting approach and a semi-implicit adaptive finite element discretization, against observed flow patterns in vesicles, which are adhered to a solid surface and are subjected to shear flow. The influence of the Gaussian curvature on the surface flow pattern is discussed.

© 2016 Elsevier Inc. All rights reserved.

1. Introduction

Lipid membranes behave as viscous fluids under physiological conditions. This interface fluidity is essential e.g. for the mobility of proteins [1], fluid domains [2] and lateral reorganizations [3]. However, even if the importance of membrane fluidity is recognized, it is only rarely accounted for in continuum modeling approaches. This might be because of the difficulty of solving, and even formulating, the governing equations for the membrane fluid flow.

The mechanics of interfacial fluids necessarily involve the tools of differential geometry, and has been formulated in various ways since the early work of Scriven [4]. As in [4] we consider a geometric formulation of the governing equations, as this highlights the tight coupling between curvature effects and interfacial hydrodynamics. We here consider an inextensible two-dimensional Newtonian fluid interface of arbitrary curvature embedded in a bulk fluid. The model can be seen as an incompressible two-phase flow problem with an inextensible Navier–Stokes equation as interface condition. Similar problems within the Stokes limit and for special geometries have been considered in [5–10]. Interfacial Navier–Stokes equations, without the coupling to the bulk fluid have been introduced in the mathematical literature by [11,12] and have been considered numerically in [13] for arbitrary but stationary interfaces and in [14] for evolving interfaces. We here focus on the coupling with the bulk fluid, but restrict the interface to be stationary. This already allows a comparison with an experiment [15] in which a vesicle was adhered to a solid surface and was subjected to a simple shear flow. The induced flow in the membrane has two vortices, which are attributable to the inextensibility of the membrane and in contrast to the toroidal circulation that would occur in the related problem of a drop of immiscible fluid attached to a surface and subject to shear [16]. The observed membrane and bulk flow patterns have already been theoretically predicted by [8,10] using a

* Corresponding author at: Institute of Scientific Computing, TU Dresden, 01062 Dresden, Germany.

E-mail address: axel.voigt@tu-dresden.de (A. Voigt).

Stokes approximation and a special hemispherical geometry of the vesicle. We will here use these results to validate our numerical approach for the full Navier–Stokes problem with arbitrary curvature.

The paper is organized as follows. After introducing the model in Section 2, we provide a diffuse interface approximation in Section 3. The numerical discretization and the validation of the model are given in Section 4. Section 5 discusses implications for more complex geometries and gives an outlook towards a full model, which also accounts for shape changes.

2. Sharp interface equations

Let Γ be a two dimensional interface separating two domains $\Omega_1 \subset \mathbb{R}^3$ and $\Omega_2 \subset \mathbb{R}^3$. The hydrodynamic equations for an incompressible fluid in the outer phase Ω_1 and the inner phase Ω_2 read

$$\begin{aligned} \partial_t \mathbf{u}_i + (\mathbf{u}_i \cdot \nabla) \mathbf{u}_i &= -\nabla p_i + \mu_i \Delta \mathbf{u}_i \\ \nabla \cdot \mathbf{u}_i &= 0 \end{aligned} \tag{1}$$

where \mathbf{u}_i is the fluid velocity, p_i the pressure and μ_i the viscosity in Ω_i . For readability, we assume the densities of the two fluids $\rho_1 = \rho_2 = 1$. Both systems of equations are coupled through the interface condition

$$\mathbf{u}_i|_{\Gamma} = \mathbf{u}_{\Gamma} \tag{2}$$

with the interfacial velocity \mathbf{u}_{Γ} on Γ . We split \mathbf{u}_{Γ} into a tangential and a normal part $\mathbf{u}_{\Gamma} = \mathbf{v}_{\Gamma} + V\mathbf{n}$, with the normal vector \mathbf{n} , but only consider stationary interfaces in this paper and thus set the normal velocity to zero, $V = 0$. The tangential part \mathbf{v}_{Γ} results as solution of the interfacial Navier–Stokes equations for an inextensible surface fluid on Γ . The equation can be derived from the Rayleigh dissipation potential [17,6]

$$W_{\Gamma} = \int_{\Gamma} \mu_{\Gamma} \left(\frac{1}{2} |\nabla_{\Gamma} \times \mathbf{v}_{\Gamma}|^2 + (\nabla_{\Gamma} \cdot \mathbf{v}_{\Gamma})^2 - K |\mathbf{v}_{\Gamma}|^2 \right) d\Gamma, \tag{3}$$

with interface viscosity μ_{Γ} , Gaussian curvature K and interface Nabla-operator ∇_{Γ} . The dynamics of the system are obtained by minimizing the potential together with the bulk contributions. For the tangential balance of linear momentum we obtain the interfacial Navier–Stokes equations [13,9,14]

$$\begin{aligned} \partial_t \mathbf{v}_{\Gamma} + (\mathbf{v}_{\Gamma} \cdot \nabla_{\Gamma}) \mathbf{v}_{\Gamma} &= -\nabla_{\Gamma} p_{\Gamma} + \mu_{\Gamma} \left(\Delta_{\Gamma}^R \mathbf{v}_{\Gamma} + 2K \mathbf{v}_{\Gamma} \right) + \mathbf{f} \\ \nabla_{\Gamma} \cdot \mathbf{v}_{\Gamma} &= 0 \end{aligned} \tag{4}$$

with the interfacial pressure p_{Γ} , which is the interface tension and serves as Lagrange multiplier to maintain the inextensibility constraint $\nabla_{\Gamma} \cdot \mathbf{v}_{\Gamma} = 0$, the Laplace–de Rham operator Δ_{Γ}^R and external forces \mathbf{f} . As in the bulk the surface material density is $\rho_{\Gamma} = 1$. Note that the surface velocity \mathbf{v}_{Γ} and the external forces \mathbf{f} in (4) are considered as three component vectors with zero normal component in the respective coordinate system $(\mathbf{e}_1(\mathbf{x}), \mathbf{e}_2(\mathbf{x}), \mathbf{n}(\mathbf{x}))$ where $\mathbf{e}_1(\mathbf{x})$ and $\mathbf{e}_2(\mathbf{x})$ denote the two basis vectors in the tangent plane at $\mathbf{x} \in \Gamma$. The force acting on an interfacial fluid surrounded by a bulk fluid is defined by the tangential part of the jump in the bulk stress tensor over the interface Γ

$$\mathbf{f} = \mathbf{P}_{\Gamma} \llbracket \mathbf{S} \mathbf{n} \rrbracket \tag{5}$$

with the projection matrix $\mathbf{P}_{\Gamma} = \mathbf{I} - \mathbf{n} \mathbf{n}^T$ and $\llbracket \mathbf{S} \mathbf{n} \rrbracket = (\mathbf{S}_2 \mathbf{n} - \mathbf{S}_1 \mathbf{n})|_{\Gamma}$, see [6] for details. The bulk stress tensor is defined by $\mathbf{S}_i = -p_i \mathbf{I} + 2\mu_i \mathbf{D}_i$ with the strain rate tensor and $\mathbf{D}_i = \frac{1}{2} (\nabla \mathbf{u}_i + \nabla \mathbf{u}_i^T)$. By using $\mathbf{P}_{\Gamma} \mathbf{n} = 0$ one can easily see that the forcing term (5) reduces to

$$\mathbf{f} = 2\mathbf{P}_{\Gamma} \llbracket \mu \mathbf{D} \mathbf{n} \rrbracket \tag{6}$$

which means that this force is independent of the bulk pressure and only considers velocity gradients. According to [13] we transform equation (4) into a stream function formulation by using the substitution $\mathbf{v}_{\Gamma} = \text{curl}(\psi)$

$$\begin{aligned} \partial_t \phi + J(\psi, \phi) &= \mu_{\Gamma} (\Delta_{\Gamma} \phi + 2\nabla_{\Gamma} \cdot (K \nabla_{\Gamma} \psi)) + \nabla_{\Gamma} \cdot (\mathbf{n} \times \mathbf{f}) \\ \phi &= \Delta_{\Gamma} \psi \end{aligned} \tag{7}$$

on Γ with the interface stream function ψ , the interface vorticity ϕ and the Jacobian $J(\psi, \phi) = -\text{curl}(\psi) \cdot \nabla_{\Gamma} \phi$. The formulation (7) has been analyzed in detail in [13] in the absence of external forces.

Summing up, the sharp interface equations of the complete system read

$$\begin{aligned} \partial_t \mathbf{u}_i + (\mathbf{u}_i \cdot \nabla) \mathbf{u}_i &= -\nabla p_i + \mu_i \Delta \mathbf{u}_i && \text{in } \Omega_i \\ \nabla \cdot \mathbf{u}_i &= 0 && \text{in } \Omega_i \\ \mathbf{u}_i|_{\Gamma} &= \text{curl}(\psi) && \text{on } \Gamma \\ \partial_t \phi + J(\psi, \phi) &= \mu_{\Gamma} (\Delta_{\Gamma} \phi + 2\nabla_{\Gamma} \cdot (K \nabla_{\Gamma} \psi)) + \nabla_{\Gamma} \cdot (\mathbf{n} \times \mathbf{f}) && \text{on } \Gamma \\ \phi &= \Delta_{\Gamma} \psi && \text{on } \Gamma \end{aligned} \tag{8}$$

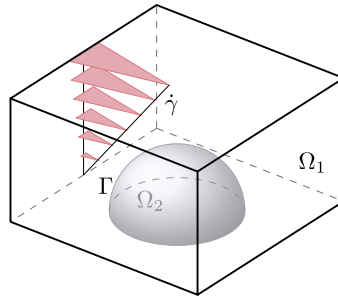


Fig. 1. Schematic computational domain Ω_1 , Ω_2 and Γ to consider the experimental setting in [15]. The red arrows indicate the shear flow through the domain and $\dot{\gamma}$ denotes the shear rate. At the bottom the vesicle is adhered to a solid wall. (For interpretation of the references to color in this figure, the reader is referred to the web version of this article.)

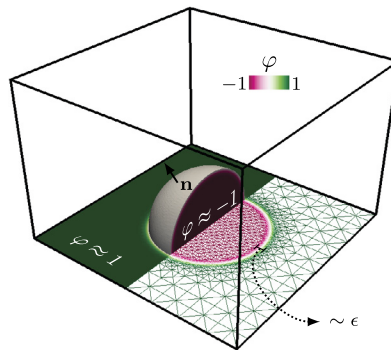


Fig. 2. Implicit description of the computational domain $\Omega = \Omega_1 \cup \Gamma \cup \Omega_2$ using a phase field function φ , together with the adaptively refined mesh. Note that the height of the bounding box is not proportional to the rest of the domain due to visual clarity.

which has to be supplemented by appropriate initial and boundary conditions. In general Γ will be a closed interface, which requires only to specify standard boundary conditions for the outer velocity \mathbf{u}_1 . However, in order to reproduce the experiment in [15], we need to consider adhesion of the interface to a solid surface, see Fig. 1. We thus specify at the solid surface $\mathbf{u}_i = 0$, as well as $\psi = 0$ and $\partial_n \psi = 0$.

3. Diffuse domain/diffuse interface approximation

To efficiently solve the coupled bulk/surface problem in eq. (8) we use a diffuse domain/diffuse interface approximation, see [18,19] for a general treatment of such problems. We consider a phase field φ to implicitly describe the interface Γ and the bulk domains Ω_i , with $\varphi \approx 1$ in Ω_1 , $\varphi \approx -1$ in Ω_2 and $\varphi \approx 0$ in Γ , e.g.

$$\varphi(\mathbf{x}) = \tanh\left(\frac{1}{\sqrt{2}\epsilon}d(\mathbf{x})\right) \tag{9}$$

with a small interface parameter $0 < \epsilon \ll 1$ defining the width of the diffuse interface and a signed distance function $d(\mathbf{x})$ describing the minimal distance of $\mathbf{x} \in \Omega$ to the interface Γ , with $\Omega = \Omega_1 \cup \Gamma \cup \Omega_2$, see Fig. 2.

The interface conditions $\mathbf{u}_i|_{\Gamma} = \text{curl}(\psi)$ are incorporated through penalty like forcing terms. Thus, the diffuse bulk Navier–Stokes equations read

$$\begin{aligned} \partial_t \mathbf{u}_i + (\mathbf{u}_i \cdot \nabla) \mathbf{u}_i &= -\nabla p_i + \mu_i \Delta \mathbf{u}_i + \mathbf{F}_i(\mathbf{u}_i, \mathbf{v}_\Gamma) \text{ in } \Omega \\ \nabla \cdot \mathbf{u}_i &= 0 \end{aligned} \tag{10}$$

with

$$\mathbf{F}_1(\mathbf{u}_1, \mathbf{v}_\Gamma) = -\frac{\beta_1}{2}(1 - \varphi)(\mathbf{u}_1 - \mathbf{v}_\Gamma), \quad \mathbf{F}_2(\mathbf{u}_2, \mathbf{v}_\Gamma) = -\frac{\beta_2}{2}(1 + \varphi)(\mathbf{u}_2 - \mathbf{v}_\Gamma)$$

with typically large penalty prefactors β_i . We use in our numerical examples $\beta_i = 10\mu_i\epsilon^{-2}$ which was justified asymptotically in [20]. We further assume that the interface velocity $\mathbf{v}_\Gamma = \text{curl}(\psi)$ is defined in the whole domain Ω and has a constant extension normal to the interface Γ . Also the surface stream function formulation eq. (7) is extended to Ω and reads

$$\begin{aligned}
 B(\varphi) (\partial_t \phi + J(\psi, \phi)) &= \nabla \cdot (B(\varphi) (\mu_\Gamma \nabla \phi + 2\mu_\Gamma K \nabla \psi + \mathbf{n} \times \mathbf{f})) \text{ in } \Omega \\
 B(\varphi) \phi &= \nabla \cdot (B(\varphi) \nabla \psi) \text{ in } \Omega
 \end{aligned}
 \tag{11}$$

where $B(\varphi) \sim (\varphi^2 - 1)^2$ defines an approximation of an interface delta function, restricting the solution to Γ , and $\mathbf{n} = \nabla \varphi / |\nabla \varphi|$. The two bulk velocities \mathbf{u}_1 and \mathbf{u}_2 allow to compute the jump in the stress tensor in the forcing term \mathbf{f} according to eq. (5), which again is extended constantly in normal direction.

Combining these equations defines a diffuse domain/diffuse interface approximation of the sharp interface equations (8), which can be justified by matched asymptotic expansions, see [21]. The coupled system reads

$$\begin{aligned}
 \partial_t \mathbf{u}_i + (\mathbf{u}_i \cdot \nabla) \mathbf{u}_i &= -\nabla p_i + \mu_i \Delta \mathbf{u}_i + \mathbf{F}_i(\mathbf{u}_i, \mathbf{v}_\Gamma) \text{ in } \Omega \\
 \nabla \cdot \mathbf{u}_i &= 0 \text{ in } \Omega \\
 B(\varphi) (\partial_t \phi + J(\psi, \phi)) &= \nabla \cdot (B(\varphi) (\mu_\Gamma \nabla \phi + 2\mu_\Gamma K \nabla \psi + \mathbf{n} \times \mathbf{f})) \text{ in } \Omega \\
 B(\varphi) \phi &= \nabla \cdot (B(\varphi) \nabla \psi) \text{ in } \Omega
 \end{aligned}
 \tag{12}$$

and combines three Navier–Stokes equations, two in the bulk phases and one in stream function formulation on the interface. Again eq. (12) has to be supplemented by appropriate initial and boundary conditions. At the solid surface we specify again $\mathbf{u}_i = 0$, as well as $\psi = 0$ and $\partial_n \psi = 0$.

4. Results

4.1. Discretization

To solve the system (12) we use a finite element approach. An operator splitting technique is applied to solve both bulk Navier–Stokes systems and the surface flow problem separately. We also use a semi-implicit Euler time stepping scheme. Let Π_h be a triangulation of Ω such that

$$\Omega_h = \bigcup_{Z \in \Pi_h} Z$$

is an interpolation of Ω . Let further T_h be a uniform partition of the time interval $(0, T]$ with end time T and time step τ . We define the discrete time derivative $d_\tau v^m = \frac{1}{\tau} (v^m - v^{m-1})$ for an arbitrary time dependent function v . The upper index denotes the time step number. The finite element spaces read

$$\begin{aligned}
 M_h &= \left\{ q \in C^0(\Omega) \cap L^2_0(\Omega) \mid q|_Z \in \mathbb{P}^r(Z) \ \forall Z \in \Pi_h \right\} \\
 V_h &= \left\{ v \in H^1_0(\Omega) \mid v|_Z \in \mathbb{P}^{r_v}(Z) \ \forall Z \in \Pi_h \right\} \\
 Y_h &= \left\{ \eta \in H^1(\Omega) \mid \eta|_Z \in \mathbb{P}^{r_\psi}(Z) \ \forall Z \in \Pi_h \right\}
 \end{aligned}$$

where $\mathbb{P}^r(Z)$ denotes the space of polynomials of degree r . on a tetrahedron $Z \in \Pi_h$. The finite element approximation of the coupled system of equations (12) now reads: find $(\mathbf{u}_{i,h}^m, p_{i,h}^m) \in V_h^3 \times M_h$ such that for all $(\mathbf{v}_i, q_i) \in V_h^3 \times M_h$

$$\begin{aligned}
 (d_\tau \mathbf{u}_{i,h}^m, \mathbf{v}_i) + ((\mathbf{u}_{i,h}^{m-1} \cdot \nabla) \mathbf{u}_{i,h}^m, \mathbf{v}_i) &= (p_{i,h}^m, \nabla \cdot \mathbf{v}_i) - (\mu_i \nabla \mathbf{u}_{i,h}^m, \nabla \mathbf{v}_i) + (\mathbf{F}_i(\mathbf{u}_{i,h}^m, \mathbf{v}_{\Gamma,h}^{m-1}), \mathbf{v}_i) \\
 (\nabla \cdot \mathbf{u}_{i,h}^m, q_i) &= 0
 \end{aligned}
 \tag{13}$$

with $\mathbf{v}_{\Gamma,h}^{m-1} = \text{curl}(\psi_h^{m-1})$, and find $(\phi_h^m, \psi_h^m) \in Y_h^2$ such that for all $(\eta, \xi) \in Y_h^2$

$$\begin{aligned}
 (B(\varphi) (d_\tau \phi_h^m + J(\psi_h^{m-1}, \phi_h^m)), \eta) &= -(B(\varphi) (\mu_\Gamma \nabla \phi_h^m + 2\mu_\Gamma K \nabla \psi_h^m + \mathbf{n} \times \mathbf{f}^m), \nabla \eta) \\
 (B(\varphi) \phi_h^m, \xi) &= -(B(\varphi) \nabla \psi_h^m, \nabla \xi),
 \end{aligned}
 \tag{14}$$

with $\mathbf{f}^m = 2\mathbf{P}_\Gamma \llbracket \mu \mathbf{D}^m \mathbf{n} \rrbracket$. A general discussion of the numerical treatment of the boundary conditions for ψ and ϕ at the solid surface is given in [22]. We consider an approach of [23], which has already been adapted to the diffuse domain/diffuse interface approximation and validated in [24]. We hereby explicitly specify $\partial_n \psi = 0$ and $\partial_n \phi = 0$ on the solid surface and treat the Dirichlet condition $\psi = 0$ implicitly using a penalty approach.

In order to ensure well-posedness of eq. (14) we replace $B(\varphi)$ by $\max(B(\varphi), \delta)$ in the second order terms with a small δ , see [18]. In our numerical examples we use $\delta = 10^{-7}$. The following simulations have been computed using the finite element toolbox AMDiS [25,26] with an adaptively refined mesh, with a high resolution along the diffuse interface, with mesh size $h \approx 3\sqrt{2}\epsilon/5$. This leads to approximately 7 to 8 points along the normal direction across the diffuse interface. Away from the diffuse interface the mesh size is much coarser but fine enough to resolve the flow properties. We use Taylor–Hood finite elements for both Navier–Stokes systems, i.e. quadratic finite elements for the velocity components and linear

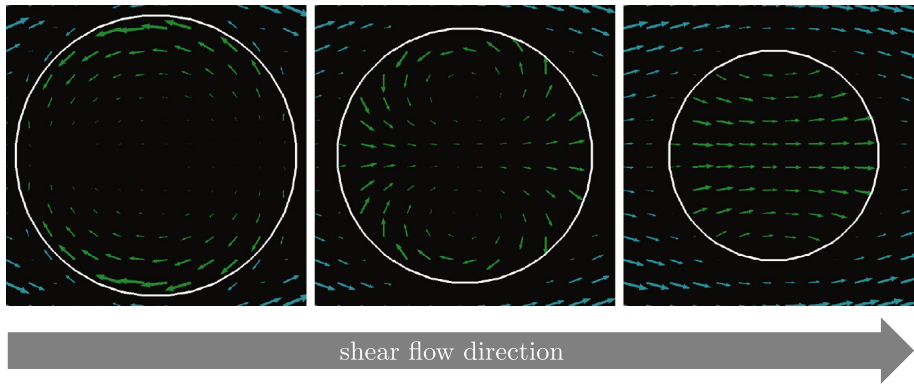


Fig. 3. Two dimensional velocity (projected to the plane and rescaled for visualization) of the sliced L_d vesicle at levels $z/R = 0.3, 0.5, 0.7$ (from left to right) for $\epsilon = 0.01$. The green arrows indicate the inner velocity \mathbf{u}_2 and the blue arrows indicate the outer velocity \mathbf{u}_1 . Shear direction: from left to right. (For interpretation of the references to color in this figure, the reader is referred to the web version of this article.)

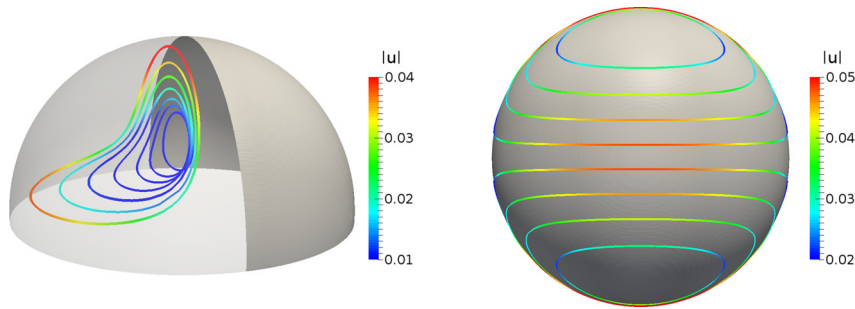


Fig. 4. Streamlines of the inner velocity \mathbf{u}_2 (left) and streamlines of the surface fluid viewed from top (right) for $\epsilon = 0.01$.

finite elements for the pressure variable. For the surface stream function formulation linear finite elements are employed. A domain decomposition approach and a parallel iterative solver BiCGStab(ell) to solve the resulting linear system enable to perform simulations with a large number of degrees of freedom with an acceptable cost.

4.2. Experimental validation

In [10] the experimental setup of [15] was used to determine membrane viscosity. Two types of vesicles – liquid ordered (L_o) and liquid disordered (L_d) – are adhered to a solid surface and are considered under shear flow. We here use the same setup to compare the experimental data as well as their proposed model and our approach. We use $\Omega = [-2l^*, 2l^*]^2 \times [0, 4l^*]$ with length scale $l^* = 20 \mu\text{m}$ as computational domain and a hemispherical geometry for the vesicle with radius $R = l^*$ located at the origin. The signed distance function used to define φ thus is $d(\mathbf{x}) = |\mathbf{x}| - R$. We consider a shear flow boundary condition with shear rate $\dot{\gamma} = \frac{1}{2} \frac{1}{t^*}$ with time scale $t^* = \frac{1}{5.2} \text{s}$ on top of Ω and no slip boundary conditions on the solid surface at the bottom. On all other boundaries we employ homogeneous Neumann conditions, which can be justified by the large spatial extension of the domain compared to the vesicle size. The bulk viscosities are set as $\mu_1 = \mu_2 = 10^{-6} \frac{\text{m}^2}{\text{s}} = 480.77 \frac{l^{*2}}{t^{*2}}$ and for the surface viscosity we use $\mu_\Gamma = 0.8736 \cdot 10^{-6} \frac{\text{m}^2}{\text{s}} = 420 \frac{l^{*2}}{t^{*2}}$ for the L_o vesicle and $\mu_\Gamma = 0.4784 \cdot 10^{-6} \frac{\text{m}^2}{\text{s}} = 230 \frac{l^{*2}}{t^{*2}}$ for the L_d vesicle. We start with zero initial condition and let the flow evolve until a steady state is reached.

Fig. 3 shows different plane cuts at different height levels through the vesicle. In Fig. 4 (left) a visualization of the inner velocity \mathbf{u}_2 is shown and in Fig. 4 (right) the streamlines of the fluid interface are shown. All these results qualitatively coincide with the experimental data in [10].

In order to compare the results quantitatively we use the velocity profile through the vesicle apex, see Fig. 5. The experimental as well as the model data, which are obtained using a Stokes approximation (black lines and black circles, respectively) are extracted from [10]. The numerical convergence of our phase field approach to the experimental data for $\epsilon \rightarrow 0$ can be observed. The velocity profile inside the vesicle, as well as the slope discontinuity at the membrane are nicely resolved. Table 1 shows the experimental order of convergence (EOC) for different norms and both vesicle types L_o and L_d . We use the L_2 norms $\|\mathbf{u} - \mathbf{v}_\Gamma\|_{2,\Gamma}$ and $\|\mathbf{u}_1 - \mathbf{u}_2\|_{2,\Gamma}$ on the interface Γ to get a measure for the approximation of the boundary conditions at the interface. In all cases a linear convergence rate is observed.

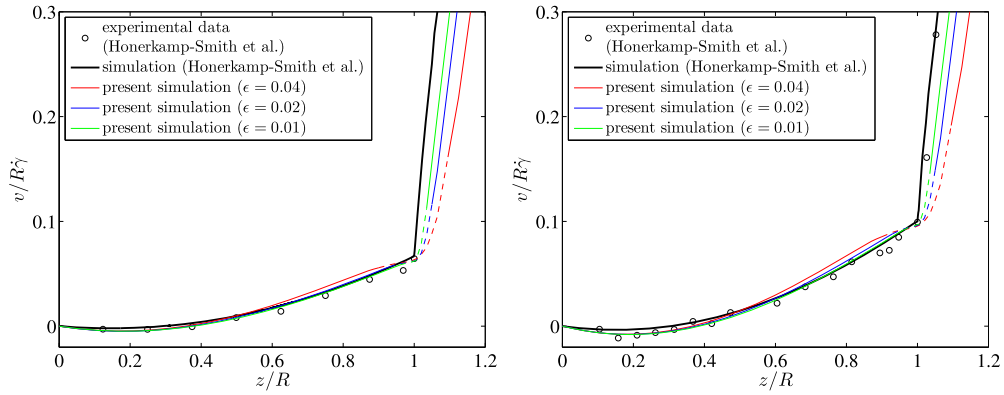


Fig. 5. Quantitative comparison of experimental/simulation data reported in [10] and the simulation of the present model for different values of ϵ and both vesicle types L_o (left) and L_d (right) where v denotes the component of the velocity field parallel to the shear flow. The dashed part of each colored lines indicates the interface region for the respective simulation. We here considered the interpolated velocity $\mathbf{u} = \frac{1}{2}((1 + \varphi)\mathbf{u}_1 + (1 - \varphi)\mathbf{u}_2)$. (For interpretation of the references to color in this figure, the reader is referred to the web version of this article.)

Table 1

Experimental order of convergence (EOC) for both L_o and L_d vesicles regarding the errors $e_1 := \|\mathbf{u} - \mathbf{v}_\Gamma\|_{2,\Gamma}$ and $e_2 := \|\mathbf{u}_1 - \mathbf{u}_2\|_{2,\Gamma}$ where $\|\cdot\|_{2,\Gamma}$ denotes the L_2 norm over the interface Γ . The mesh size h within the diffuse interface is related to the interface width ϵ by $h \approx 3\sqrt{2}\epsilon/5$.

ϵ	L_d vesicle				L_o vesicle			
	e_1	EOC	e_2	EOC	e_1	EOC	e_2	EOC
0.10	0.0142	–	0.0145	–	0.0142	–	0.0145	–
0.09	0.0124	1.298	0.0127	1.289	0.0123	1.304	0.0126	1.295
0.08	0.0112	0.818	0.0115	0.829	0.0112	0.823	0.0115	0.836
0.07	0.0101	0.767	0.0103	0.778	0.0101	0.771	0.0103	0.783
0.06	0.0089	0.818	0.0091	0.829	0.0089	0.817	0.0091	0.829
0.05	0.0079	0.691	0.0080	0.702	0.0078	0.696	0.0080	0.709
0.04	0.0063	1.006	0.0064	1.007	0.0063	1.014	0.0064	1.017
0.03	0.0050	0.824	0.0050	0.828	0.0049	0.829	0.0050	0.835
0.02	0.0033	1.005	0.0034	0.999	0.0033	1.010	0.0033	1.009
0.01	0.0017	0.991	0.0017	0.973	0.0016	0.998	0.0017	0.992

5. Summary and outlook

5.1. Ellipsoidal shaped vesicle

As our approach is not limited to a hemispherical shape we consider an ellipsoidal shape for the vesicle. The ellipsoid is characterized by the zero level set of the function $q(\mathbf{x}) = \mathbf{x}^T A^2 \mathbf{x} - 1$ with the diagonal coefficient matrix $A = \text{diag}(\mathbf{a}) \in \mathbb{R}^{3 \times 3}$ and $\mathbf{a} = (a_0^{-1}, a_1^{-1}, a_2^{-1})^T$. The function $q(\mathbf{x})$ can easily be transformed into a signed distance function $d(\mathbf{x})$ using coordinate transformations. In the following simulations we use the coefficients $a_0 = 0.8l^*$, $a_1 = 1.2l^*$ and $a_2 = 0.9l^*$ and rotate the ellipsoid around the z -axis (height axis) by an angle of $\pi/5$ to break the symmetry. As for the hemispherical vesicle, also the ellipsoid is in equilibrium if the volume $|\Omega_2|$ is conserved and the membrane is inextensible. So also for this configuration our assumption of a stationary profile is fulfilled. All other parameters remain. We consider a L_d vesicle.

We visualized the inner flow field in Fig. 6 (top row) in form of plane cuts at different height levels through the vesicle. In contrast to a hemisphere as used in the prior sections the ellipsoidal shape has a non constant Gaussian curvature K (see Fig. 6) and therefore a direct influence on the surface flow field. The influence of the geometry on the flow field can be analyzed by an effective geometric interaction which depends linearly on the geometric potential U defined by the surface Laplace equation $\Delta_\Gamma U = K$, see [27,14] for details. Due to this interaction, vortices in a flow field are typically attracted to peaks and valleys, i.e. local maxima of the Gaussian curvature. The steady state interfacial flow field is shown in Fig. 6 (bottom row, left) in form of the surface streamlines. The two vortices are shifted towards the regions of high Gaussian curvature K , see Fig. 6 (bottom row, center and right), which shows the Gaussian curvature K and the geometric potential U for the ellipsoidal shaped vesicle. However, already the specified no-slip boundary condition on the substrate prohibit the vortices to be located at the points of highest Gaussian curvature. Furthermore, the surface flow field is influenced by the bulk flow. So, if this shift in location of the vortices is a result of the geometric potential or has its origin in the bulk flow or the specified boundary conditions remains open. To identify the effect we vary the geometry. We thereby keep the height of the ellipsoid $a_2 = 0.9l^*$ constant to have a comparable interaction with the bulk flow. Furthermore, we fix the area of the ellipsoid, to maintain comparable surface flow properties. We only vary a_0 and a_1 , see Fig. 7.

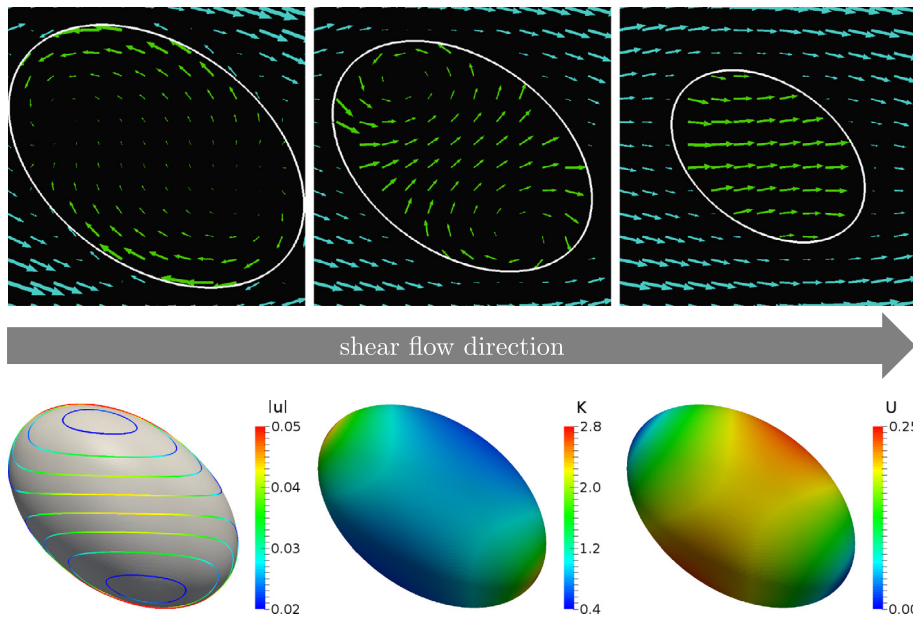


Fig. 6. Top row: Two dimensional velocity (projected to the plane and rescaled for visualization) for the sliced ellipsoidal vesicle at levels $z = 0.3, 0.5, 0.7$ (from left to right) for $\epsilon = 0.01$. The green arrows indicate the inner velocity \mathbf{u}_2 and the blue arrows indicate the outer velocity \mathbf{u}_1 . Bottom row: Streamlines of the surface fluid (left), Gaussian curvature K (center) and the geometric potential U (right) viewed from top for the ellipsoid and $\epsilon = 0.01$. Shear direction: from left to right. (For interpretation of the references to color in this figure, the reader is referred to the web version of this article.)

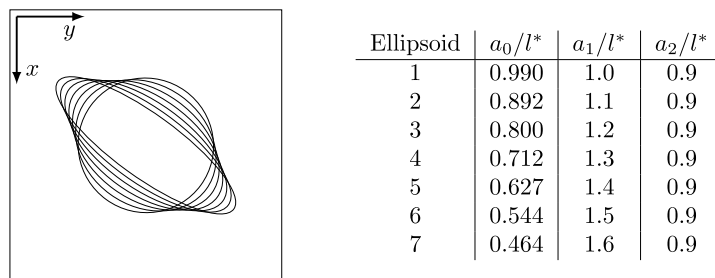


Fig. 7. Considered ellipsoidal shapes visualized as contour lines of the phase field function in the bottom plane (left) and table with axis parameter for the considered ellipsoids (right).

Fig. 8 shows the setting, with the red dot the center of one vortex and the blue dot the point of highest curvature on the major axis. We measure the geodesic distance d between both points. The value should decrease with increasing curvature effect. In **Fig. 9** d is plotted for different geometries in comparison with the results, which would be obtained without the Gaussian curvature term in the surface Navier–Stokes equation. The value decreases for more elongated ellipsoids and also the difference between the results with the correct K and with $K = 0$ increases, which indicates the geometric contribution.

5.2. Outlook

We have introduced a model for a stationary fluidic interface in a viscous fluid. The interface is treated as lower dimensional surface since its thickness is much smaller than its lateral extension. The interfacial hydrodynamics can be described by the surface Navier Stokes equations [6] – a generalization of the Navier Stokes equation in the two dimensional plane. In order to prevent dealing with vector fields and local coordinates on general surfaces we used the surface stream function formulation introduced in [13,14]. This formulation allows using standard numerical techniques for surface PDEs. The basic ideas of [18] and [19] are used to transform the model in a description with phase fields. We have validated the model on the experimental data provided in [10] and have shown the numerical convergence of our approach for the interface parameter $\epsilon \rightarrow 0$. Additionally, we have presented numerical examples for interfaces with non constant Gaussian curvature K and the interaction with the underlying geometry. The numerical approach is reliant on the inextensibility of the membrane. Without this constraint simplified models can be built which consider the membrane fluidity implicitly using a Boussinesq–Scriven interface stress tensor, see e.g. [28–31]. The resulting interfacial flow patterns in these models, which consider droplets instead of vesicles or cells, are qualitatively different and lead to toroidal circulation [16].

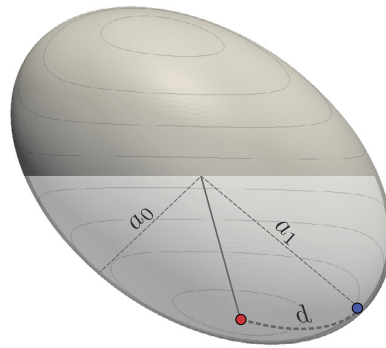


Fig. 8. Ellipsoidal surface with surface stream lines, the center of one vortex (red dot) and highest curvature point (blue dot), the major and minor axis of the projected ellipsoid, and the measured values d . (For interpretation of the references to color in this figure, the reader is referred to the web version of this article.)

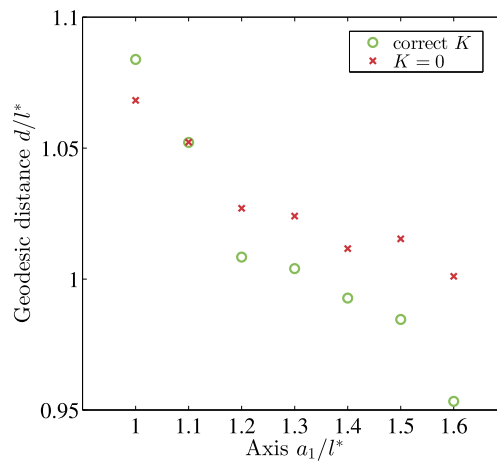


Fig. 9. The geodesic distance d as a function of the major axis of the ellipsoid. In addition the results for $K = 0$ in the surface Navier–Stokes equation are shown for comparison for the same geometries.

The coupling of surface hydrodynamics and bulk flow is of special interest for spinodal decomposition in lipid bilayer membranes. A description for planar lipid bilayer membranes can be found in [32]. Our approach is not restricted to special geometries and can be applied for a broad range of surfaces if a smooth phase field function φ is provided. The model can be used to investigate spinodal decomposition on general surfaces under the influence of bulk flow. Furthermore, an extension to moving surfaces is possible. This has already been considered for the interfacial hydrodynamic equations in [14]. With this extension further physical effects of lipid bilayer membranes can be taken into account such as bending or spontaneous curvature effects, which have already been considered within a phase field context, under the inextensibility constraint, but without membrane fluidity [33–35]. To combine these approaches will be subject of future work.

Acknowledgement

This work was supported by DFG within SPP 1506 through Vo899/11-2. We would like to thank Sebastian Aland for fruitful discussions and his support. We further acknowledge the provided computing resources at JURECA at JSC Jülich and at TAURUS at ZIH/TU Dresden.

References

- [1] P.G. Saffman, M. Delbrück, Brownian motion in biological membranes, *Proc. Natl. Acad. Sci.* 72 (8) (1975) 3111–3113.
- [2] P. Cicuta, S.L. Keller, S.L. Veatch, Diffusion of liquid domains in lipid bilayer membranes, *J. Phys. Chem. B* 111 (13) (2007) 3328–3331.
- [3] K. Simons, W.L.C. Vaz, Model systems, lipid rafts, and cell membranes, *Annu. Rev. Biophys. Biomol. Struct.* 33 (2004) 269–295.
- [4] L.E. Scriven, Dynamics of a fluid interface equation of motion for Newtonian surface fluids, *Chem. Eng. Sci.* 12 (2) (1960) 98–108.
- [5] M.L. Henle, R. McGorty, A.B. Schofield, A.D. Dinsmore, A.J. Levine, The effect of curvature and topology on membrane hydrodynamics, *Europhys. Lett.* 84 (4) (2008) 48001.
- [6] M. Arroyo, A. DeSimone, Relaxation dynamics of fluid membranes, *Phys. Rev. E* 79 (2009) 031915.
- [7] M.L. Henle, A.J. Levine, Hydrodynamics in curved membranes: the effect of geometry on particulate mobility, *Phys. Rev. E* 81 (2010) 011905.
- [8] F.G. Woodhouse, R.E. Goldstein, Shear-driven circulation patterns in lipid membrane vesicles, *J. Fluid Mech.* 705 (2012) 165–175.

- [9] M. Rahimi, A. DeSimone, M. Arroyo, Curved fluid membranes behave laterally as effective viscoelastic media, *Soft Matter* 9 (2013) 11033–11045.
- [10] A.R. Honerkamp-Smith, F.G. Woodhouse, V. Kantsler, R.E. Goldstein, Membrane viscosity determined from shear-driven flow in giant vesicles, *Phys. Rev. Lett.* 111 (2013) 038103.
- [11] D.G. Ebin, J. Marsden, Groups of diffeomorphisms and the motion of an incompressible fluid, *Ann. Math.* 92 (1) (1970) 102–163.
- [12] M. Mitrea, M. Taylor, Navier–Stokes equations on Lipschitz domains in Riemannian manifolds, *Math. Ann.* 321 (4) (2001) 955–987.
- [13] I. Nitschke, A. Voigt, J. Wensch, A finite element approach to incompressible two-phase flow on manifolds, *J. Fluid Mech.* 708 (2012) 418–438.
- [14] S. Reuther, A. Voigt, The interplay of curvature and vortices in flow on curved surfaces, *Multiscale Model. Simul.* 13 (2) (2015) 632–643.
- [15] C. Vezy, G. Massiera, A. Viallat, Adhesion induced non-planar and asynchronous flow of a giant vesicle membrane in an external flow, *Soft Matter* 3 (2007) 844–851.
- [16] E.B. Dussan V., On the ability of drops to stick to surfaces of solids. Part 3. The influences of the motion of the surrounding fluid on dislodging drops, *J. Fluid Mech.* 174 (1987) 381–397.
- [17] G. Dörries, G. Foltin, Energy dissipation of fluid membranes, *Phys. Rev. E* 53 (1996) 2547–2550.
- [18] A. Rätz, A. Voigt, PDE's on surfaces: a diffuse interface approach, *Commun. Math. Sci.* 4 (3) (2006) 575–590.
- [19] X. Li, J. Lowengrub, A. Rätz, A. Voigt, Solving PDEs in complex geometries: a diffuse domain approach, *Commun. Math. Sci.* 7 (1) (2009) 81–107.
- [20] S. Franz, H.-G. Roos, R. Gärtner, A. Voigt, A note on the convergence analysis of a diffuse-domain approach, *Comput. Methods Appl. Math.* 12 (2) (2012) 153–167.
- [21] K.E. Teigen, X. Li, J. Lowengrub, F. Wang, A. Voigt, A diffuse-interface approach for modeling transport, diffusion and adsorption/desorption of material quantities on a deformable interface, *Commun. Math. Sci.* 7 (2009) 1009–1037.
- [22] W. E, J.-G. Liu, Vorticity boundary condition and related issues for finite difference schemes, *J. Comput. Phys.* 124 (2) (1996) 368–382.
- [23] D. Calhoun, A Cartesian grid method for solving the two-dimensional streamfunction-vorticity equations in irregular regions, *J. Comput. Phys.* 176 (2) (2002) 231–275.
- [24] K. Padberg-Gehle, S. Reuther, S. Praetorius, A. Voigt, Transfer operator-based extraction of coherent features on surfaces, in: *Topological Data Analysis*, Springer (to appear).
- [25] S. Vey, A. Voigt, AMDiS: adaptive multidimensional simulations, *Comput. Vis. Sci.* 10 (1) (2007) 57–67.
- [26] T. Witkowski, S. Ling, S. Praetorius, A. Voigt, Software concepts and numerical algorithms for a scalable adaptive parallel finite element method, *Adv. Comput. Math.* 41 (2015) 1145–1177.
- [27] A.M. Turner, V. Vitelli, D.R. Nelson, Vortices on curved surfaces, *Rev. Mod. Phys.* 82 (2010) 1301–1348.
- [28] J.T. Schwalbe, F.R. Phelan Jr., P.M. Vlahovska, S.D. Hudson, Interfacial effects on droplet dynamics in Poiseuille flow, *Soft Matter* 7 (2011) 7797–7804.
- [29] A. Reusken, Y. Zhang, Numerical simulation of incompressible two-phase flows with a Boussinesq–Scriven interface stress tensor, *Int. J. Numer. Methods Fluids* 73 (12) (2013) 1042–1058.
- [30] J.W. Barrett, H. Garcke, R. Nürnberg, Stable numerical approximation of two-phase flow with a Boussinesq–Scriven surface fluid, *Commun. Math. Sci.* 13 (2015) 1829–1874.
- [31] J. Gounley, G. Boedec, M. Jaeger, M. Leonetti, Influence of surface viscosity on droplets in shear flow, *J. Fluid Mech.* 791 (2016) 464–494.
- [32] J. Fan, T. Han, M. Haataja, Hydrodynamic effects on spinodal decomposition kinetics in planar lipid bilayer membranes, *J. Chem. Phys.* 133 (23) (2010) 235101.
- [33] T. Biben, C. Misbah, Tumbling of vesicles under shear flow within an advected-field approach, *Phys. Rev. E* 67 (2003) 031908.
- [34] A. Laadhari, P. Saramito, C. Misbah, Vesicle tumbling inhibited by inertia, *Phys. Fluids* 24 (3) (2012) 031901.
- [35] S. Aland, S. Egerer, J. Lowengrub, A. Voigt, Diffuse interface models of locally inextensible vesicles in a viscous fluid, *J. Comput. Phys.* 277 (2014) 32–47.